On Efficient UHF RFID Coverage inside a Room

Antonis G. Dimitriou[#], Aggelos Bletsas[+], Anastasis C. Polycarpou[*], John N. Sahalos[°]

[#] *Department of Electrical & Computer Engineering, Aristotle University of Thessaloniki*
AUTh Campus, ECE Dept., 54124, Thessaloniki, Greece
antodimi@ee.auth.gr

[+] *Department of Electronic & Computer Engineering, Technical University of Crete*
TUC Campus, Kounoupidiana, 73100, Chania, Greece
aggelos@telecom.tuc.gr

[*] *Department of Engineering, University of Nicosia,*
Makedonitissas Ave. 46, 1700, Nicosia, Cyprus
polycarpou.a@unic.ac.cy

[°] *Physics Department, Aristotle University of Thessalonik,*
AUTh Campus, RCLab, 54124, Thessaloniki, Greece
sahalos@auth.gr

***Abstract*— This paper investigates the problem of improving the identification performance of a UHF RFID system inside a room. We assume static reader, passive tags and availability of commodity antennas. In sharp contrast to prior art that has focused on free space or simple two-ray model, a ray-tracing propagation model is developed that includes multipath in 3D space. It is found that careful selection of reader antenna placement and tilting must be performed to control destructive interference effects. Furthermore, 3D coverage performance gains on the order of 10% are observed by implementing tags' diversity. Finally, a device that successfully manipulates destructive interference is introduced.**

I. Introduction

Radio Frequency Identification (RFID) is widely adopted in several applications including asset management, product tracking, logistics, inventory systems, security, location-based services and many more. UHF RFID systems have extended the identification-range of the original LF or HF RFID systems. Depending on the type of tags implemented, a UHF EPC Gen2 operating RFID reader can identify "passive" tags within a few metres or "active" tags within tens of metres. Despite the wide spread of the technology and the importance of accurate read-region estimations, read-region is usually defined from simplistic free-space equations [1]—[3]. The site-specific nature of propagation has been neglected, while the problem of planning an operational RFID network of readers has been overlooked.

In this paper, we treat the problem of maximizing the coverage of a UHF RFID system operating inside a single room with commodity RFID hardware. This represents part of a greater project that includes the design and implementation of a pilot RFID system inside a hospital [4]. Passive tags are attached to medical equipment, such as infusion pumps and wheelchairs inside a room. Our goal is to maximize the identification percentage within a given volume of interest, as demonstrated in Fig. 1.

We developed a ray-tracing model, capable of including the complex environment in the estimations process. The field inside the volume of interest is calculated as the superposition of several contributions arriving from diverse propagation paths. The radiation pattern and the polarization of the reader's antennas as well as the tags' antennas, the frequency of operation, the constitutive parameters of the walls and the transmission power are considered. Conclusions are derived on antenna selection, antenna placement and orientation, tags' diversity.

Finally, we propose the introduction of a switch-controlled phase shifter in the feeding of a double antenna configuration, capable of minimizing destructive-interference effects and thus, boosting coverage performance and system reliability.

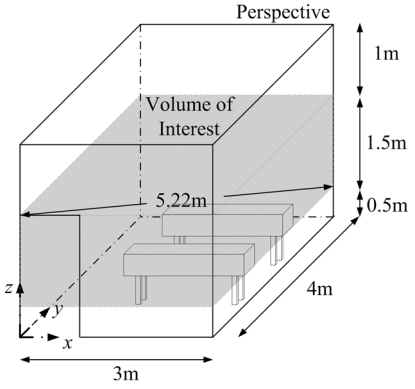

Fig. 1 Room representation with volume of interest.

II. Propagation Model

A ray-tracing model [5], including the direct and the multiply reflected fields at each location is developed. Proper algorithms for the manipulation of vectors and their transformations among different Spherical and Cartesian coordinate systems have been realised.

For a linearly polarized antenna, the magnitude at distance r of the radiated wave electric far-field component E_{inc} is given by:

$$E_{inc} = \sqrt{\frac{\eta P_t G_t(\theta,\phi)}{2\pi}}\frac{1}{r} \qquad (1)$$

P_t is the transmission power in Watts, $G_t(\theta,\varphi)$ is the antenna's gain at angles θ, φ and η is the free-space impedance. In order to model a circularly polarized antenna, another field vector, orthogonal to the above with a π phase delay and its corresponding radiation pattern is considered.

For each reflection, the incident field on the boundaries of a wall is analyzed in two orthogonal vectors; one parallel to the plane of incidence and one perpendicular. Then, the reflection coefficients are calculated, by employing the recursive formulation presented in [6]. A uniform plane wave incident at an oblique angle upon N layers of planar dielectric slabs that are bordered on either side by free space is considered. The constitutive parameters of the wall are taken into account by selecting the permittivity and the loss tangent of each layer [7]—[8]. Each reflection might lead to a different phase shift and magnitude-change of the vertically and the horizontally polarized components of the incident field respectively, thus leading to a change in the polarization state of the reflected field with respect to that of the incident field.

Each ray is traced until it reaches the receiving position. At the receiver, the field from each path is decomposed in three orthogonally arranged axes x, y, z. Assuming that the electric field's component of the i^{th} ray along the tag's polarization axis is E_i^{tag}, the total field at the tag's antenna is given as the phase sum of all contributions:

$$E^{tag} = \sum_{i=1}^{N} \sqrt{G^{tag}\left(\theta_i^{tag},\phi_i^{tag}\right)} E_i^{tag} e^{j(2\pi ft + 2\pi r_i/\lambda + \varphi_i)}, \qquad (2)$$

where r_i is the distance traveled by the i^{th} ray and φ_i is the phase shift of the specific contribution, due to the reflections on the surrounding walls, $G^{tag}\left(\theta_i^{tag},\phi_i^{tag}\right)$ is the gain of the tag's antenna at the angle-of-arrival $\theta_i^{tag},\phi_i^{tag}$ measured at a spherical coordinate system centred at the tag and λ is the wavelength of operation.

Finally, the power at the tag's chip P_{tag} is given as:

$$P_{tag} = \frac{\lambda^2}{4\pi}\frac{E_{tag}^2}{2\eta}\tau, \quad (4)$$

where τ is the power transmission coefficient, expressing mismatches between the chip's impedance $Z_c=R_c+jX_c$ and the antenna's impedance $Z_a=R_a+jX_a$:

$$\tau = \frac{4R_cR_a}{\left|Z_c+Z_a\right|^2}, \quad 0 \le \tau \le 1 \quad (5)$$

Such detailed model represents the foundation for accurate characterization of the multipath profile, and allows the development of techniques that control interference effects, as demonstrated later.

III. Definition of Coverage

Literally, a point in space is considered covered, if the modulated backscattered field (from a passive tag at that point) reaches the reader with sufficient power, i.e. with power above reader's sensitivity threshold. In the case of passive UHF RFID tags, as examined herein, the radiated power from the reader's antenna is needed to power up the tag's IC that employs a rectifier circuit [9]. Typically, tag-to-reader communication is binary modulated, with conjugate match of tag's antenna to the IC chip in the first state and optimized tag's design in the second state [10]; if the incident power is sufficient to power up the tag's IC, then the back-scattered power at the reader is typically much greater than its sensitivity level [11]. Therefore, identification is accomplished if the tag is powered up and coverage in this work depends on the required minimum power to activate tag's chip. This quantity is calculated in (4).

The corresponding measured power sensitivity of two major UHF Gen2 RFID chips varied between -11.5dBm and -12.5dBm [11]. Significantly improved sensitivity values have been reported recently by major manufacturers, ranging from -15dBm [12], [13] down to -18dBm [14]. However, it must be emphasized that the nominal threshold may not be accomplished in the entire operating frequency band, due to the variation of the tag IC impedance with frequency. Also, depending on the material where the tag is attached to, one should expect a gain loss [15] ranging from 1dB (for paper or acrylic) up to more than 10dBs for aluminum surfaces, where specialized tags need to be designed.

It is desired not to restrict the analysis in the following sections to a specific tag, but to include important parameters of the problem, like polarization. We calculate the received power, using the analytical ray-tracing model described in (1)—(5), along three orthogonally arranged axes x, y, z, thus taking into account the polarization state of the incident field with respect to that of the tag's antenna, on the tips of a cubic grid. The radiation pattern of the tag's antenna is considered omni-directional with 0dBi gain, in order not to favour specific directions-of-arrival of the different field's components; the transmission coefficient τ is assumed equal to 1. A tag is considered "identified" if the power at the polarization axis of the tag is greater than the tag's threshold.

Thus, for a given tag's threshold, we can estimate the coverage percentage, or identification percentage, in any area or volume of interest and for any polarization of the tag's antenna, including circular polarization or polarization-diversity by evaluating the ratio of the points identified N_{id} over the total number of gridpoints N_{tot}: N_{id}/N_{tot}. Some representative results are given in Fig. 4, for a z-polarized tag at three different heights inside the room as well as in the entire volume of interest (Fig. 1). The tag's threshold is varied from -14dBm up to -4dBm. These results are presented in the following section.

IV. Estimation Results

The target is to maximize the coverage percentage within a volume of interest inside a room, as demonstrated in Fig. 1. The available antennas are manufactured by "MTI Wireless". The tags are expected to be both horizontally as well as vertically attached to the objects of interest, depending on geometry of the latter. In order to transmit power polarized along the horizontal and the vertical plane, circularly polarized transmitting antennas have been selected. One is the "MT-242017/NRH" with 10dBic gain and dimensions equal to

37cm×37cm and the other is the "MT-242032/NRH" with 7dBic gain and dimensions 19cm×19cm.

Initially, some characteristic results are demonstrated. The "MT-242017/NRH" antenna is considered at the position shown in Fig. 2, properly tilted, so as to illuminate the volume of interest. The transmission power is set to 30dBm at the frequency of 865MHz. The vertical walls and the ceiling are modeled as reinforced concrete walls [7] with ε_r=6.5 and tanδ=0.287. The floor is modeled as "wet ground" with ε_r=30 and tanδ=0.103 [8]. The power is calculated in the entire room on the tips of a cubic grid spaced by 10cm. The received power along an *x*-slice (Fig. 2) at *x*=2.5m for a *z* polarized tag is given in Fig. 3. Similar results can be extracted for any polarization axis and for any cut. By combining these results, one can recognize the dominant propagation mechanisms, responsible for the field's interference patterns inside the room due to multipath and then properly move the antenna inside the room, manipulating the resulting field as desired.

As discussed in the previous section, coverage plots are formed by processing the power results. In Fig. 4, the coverage results for a *z* polarized tag for increasing tag's threshold are given. Coverage curves are given in three selected heights, at 0.5m, 1.2m and 1.8m above the ground, as well as aggregate results in the entire volume of interest (shown in Fig. 1). Coverage performance is calculated at different heights, as we seek for balanced performance in the entire volume of interest. Similar plots are yielded for all polarization axes.

A. Tags' Diversity

In the introduction it was mentioned that asset tracking involves wheelchairs and infusion pumps. Benefiting from the tags' low cost and small dimensions, combined with the tracked-objects' large dimensions, we can associate more than a single tag with each object. To examine this case of diversity, we assume three tags polarized at x, y and z directions respectively, attached to each object. In each location, successful identification is guaranteed if at least one of the tags is powered up. The coverage performance assuming three orthogonally arranged tags at each location is shown in Fig. 5. Aggregate coverage increases by 10% at the -14dBm threshold, reaching 89%, compared to the single *z*-polarized-tag case shown in Fig. 4. Even better improvement is recorded at greater tag's threshold.

B. Actual Field vs. Free-Space Estimation

In the related literature, read-region is defined by the simplistic Friis free-space equation or at best the two-ray model, accounting only for ground reflections [1]. Recently, in [2], the authors attempt to include multipath in the performance of a UHF RFID system, by considering a stochastic model to describe the variations of the field around a mean value that is estimated based on a simple two-slope path-loss model. On the contrary, this work is one of the first in the literature (to the best of our knowledge) that implements a realistic, site-specific multipath model for RFID coverage performance evaluation.

For the same configuration shown in Fig. 2, we calculate the field inside the room, assuming free-space conditions. By comparing the coverage performance of the two cases in Fig. 6, assuming tags' diversity as discussed in the previous paragraph, better coverage is accomplished when considering the actual field. This is easily explained as follows: the mean expected power at each receiving location is greater than the power in Free-space conditions, because in the geometry examined herein a) the direct contribution is never obstructed, and b) the "Reflected Field", due to the surrounding walls is added to the direct field, thus raising the mean expected power.

The problem in the real environment, due to multipath, is the reliability of the coverage at any given point. At "free-space" conditions a position is covered depending only on the transmitted power and the radiation patterns of the two antennas. In the "real room" coverage depends on the phase and magnitude relations of the different contributions, causing the creation of "coverage-holes" even at the vicinity of the antenna, due to destructive interference. In section V, a device is proposed that reduces such effects.

C. One vs. Two Reader Antenna Configuration

By considering any of the available transmitting antennas, at several configurations inside the room (different walls, center or corner, different tilting), part of the volume of interest to the left or to the right of the antenna could not be covered, due to the narrow 3dB beamwidth of the horizontal radiation patterns of the two antennas.

To overcome this limitation, five different double antennas configurations were tested. Two of these setups that reveal important properties of the field inside the room are demonstrated in Figs. 7—8. The two antennas are fed via a 3dB bi-directional power splitter/combiner and both transmit the same signal. As a result, each antenna transmits at 3dB smaller power level (27dBm) than in the single-antenna configurations. Hence, a fair comparison with the single antenna configurations can be carried out, given that the same amount of power is radiated inside the room. In addition, as the antennas were to be installed inside a patient's room, the "MT-242032/NRH" with 7dBic gain antennas were selected, due to their significantly reduced dimensions, compared to the 10dBic antenna. The EIRP per antenna and per excitation axis is 31dBm; much smaller than the maximum limit in Europe.

Fig. 9 shows the power along a *z*-slice at 1.2m for a *z*-polarized tag for "Configuration 1" (Fig. 7). The hyperbolas, drawn in Fig. 9, represent the geometric-space of the points in the room with distances from the two sources d_1, d_2 respectively, such that the direct fields from the two antennas contribute with π phase difference, hence add destructively. Depending on the magnitude of each direct contribution, the minimum could be so large, that a tag at this location could not be identified, despite of its small distance from the two antennas. Therefore, in this case, the two antennas form an antenna-array, creating minima at predictable locations.

Returning to the problem of maximization of coverage in the volume of interest (Fig. 1), it was desired *a*) to minimize destructive interference effects, caused by the two antennas,

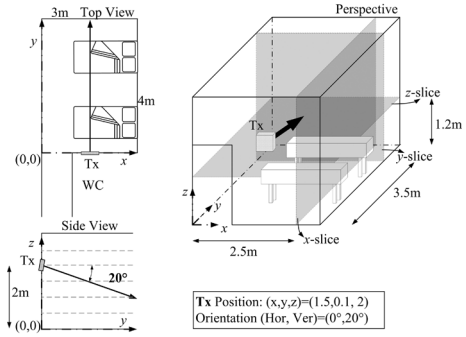

Fig. 2 Representation of a single antenna configuration in top view and side view.

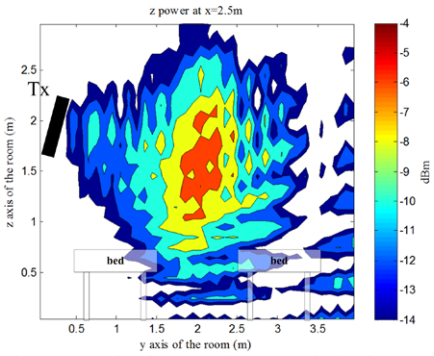

Fig. 3 Received power for a z-polarized tag at x=2.5m.

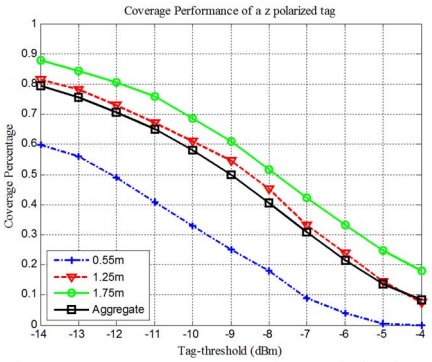

Fig. 4 Coverage percentage of a z-polarized tag for increasing tag's threshold.

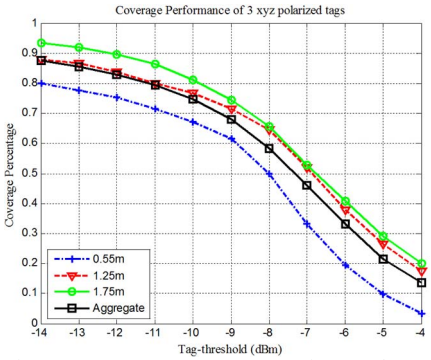

Fig. 5 Coverage percentage, assuming 3 orthogonally polarized tags at each location.

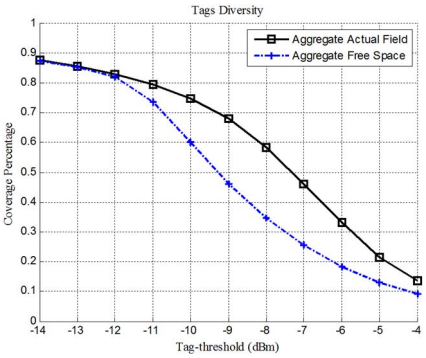

Fig. 6 Coverage performance assuming free space conditions vs. the actual field, considering 3 orthogonally polarized tags at each location.

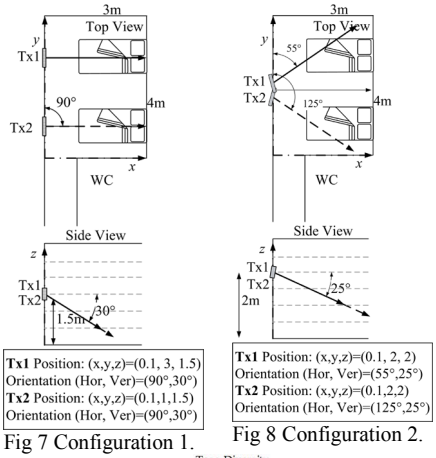

Fig 7 Configuration 1.

Fig 8 Configuration 2.

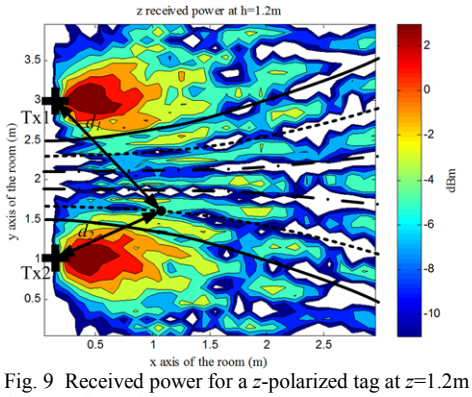

Fig. 9 Received power for a z-polarized tag at z=1.2m for "Configuration 1".

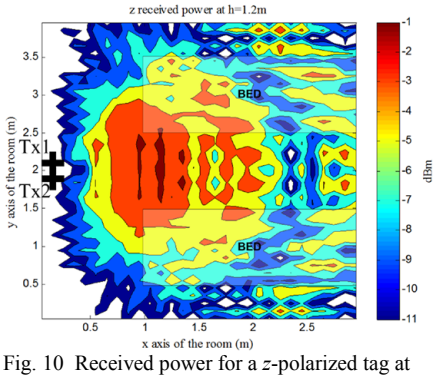

Fig. 10 Received power for a z-polarized tag at z=1.2m for "Configuration 2".

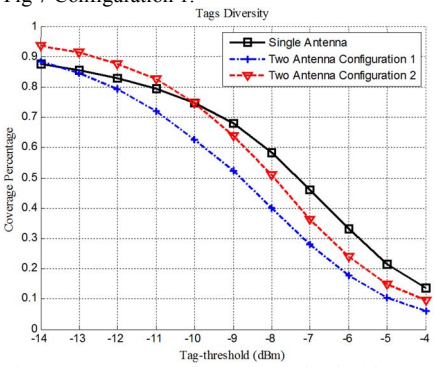

Fig. 11 Coverage performance of the double antenna configurations vs. the single antenna one.

while *b*) radiating power towards the desired volume. These constraints are well satisfied by "Configuration 2" shown in Fig. 8. The two antennas illuminate different parts of the room, so that the 3dB horizontal beamwidths of each of the antennas radiate at different angular segments. A z-slice at 1.2m of the z-polarized received power is shown in Fig. 10.

The coverage performance of the two configurations of Fig. 7 is shown in Fig. 11, assuming tags' diversity. "Configuration 2" ensured 93% coverage at -14dBm. By comparing the coverage performance of "Configuration 2" with the corresponding one for the single antenna configuration, shown in Fig. 2, better coverage percentage is accomplished at the expected tags' thresholds, as demonstrated in Fig. 11, despite the fact that each of the two antennas radiates at 3dB smaller power level. The reason is that the transmitted power is better directed towards the volume of interest.

V. Introducing a Phase-Shifter

Despite the fact that 93% coverage was accomplished with a double antenna configuration, fed via a 3dB splitter, it was found that the remaining 4 double antenna configurations suffer from destructive interference effects, causing severe degradation of the coverage performance of the system. Directing the power towards the volume of interest is not a sufficient condition for effective planning. Control of destructive-interference effects represents an equally important

parameter of the problem. In addition, the expected coverage-performance remains vulnerable to technician's installation errors.

As discussed earlier, the two antennas behave as an array introducing "holes" in the surrounding area based on the magnitude and the phases of the transmitted fields. The desired effect is to "control" the locations of the holes and properly "move" them inside the room.

We propose the selective introduction of a phase-delay in the feeding path of one of the antennas controlled by an electronic switch (Fig. 12). A switch controls feeding of one of the antennas, either with zero phase delay (hence the two antennas radiate in phase) or introducing a π phase delay. Thus in the two states of the switch the "holes" in the room are displaced since destructive interference occurs at different positions inside the room and the coverage performance of the system is boosted. The proposed device can only manipulate destructive interference caused by the destructive sum of contributions from different antennas and not those minima, caused due to the field originated by the same antenna (e.g. due to scattering).

In five different configurations, including 3 setups not shown, where coverage was as low as 76%, identification is increased above 93% with tags' diversity (Fig. 13). Another important benefit of the introduction of the phase-shifter is that the system can tolerate technicians' installation errors. The planning rule is simplified to "directing the energy towards the area of interest", while "maintaining some interaction between the two antennas", in order to produce switch-controlled interference patterns.

VI. Conclusions

A ray-tracing site specific propagation model has been developed for accurate UHF RFID systems' planning. Coverage optimization inside a single room for a static RFID reader, assuming only passive tags was investigated. The problem has been treated in a 3 dimensional volume. It was shown that tags' diversity can greatly enhance the identification percentage of the system. Careful reader antenna placement must be performed in order to minimize destructive interference effects caused by the surrounding environment. When several antennas are used, additional interference effects due to the phase-sum of the fields from the antennas are inserted. Destructive interference effects create minima even at the vicinity of the antennas and should be controlled. We propose the introduction of a switch controlled phase shifter in the feeding of one of the antennas in order to displace the locations of the coverage holes in the two states of the switch, thus increasing the reliability and the coverage performance of the system.

Acknowledgement

This research is funded by the Cyprus Research Promotion Foundation grant ΤΠΕ/OPIZO/0308(BIE)/13.

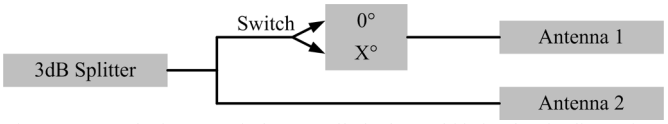

Fig. 12 Introducing a switch controlled phase-shift in the feeding of one antenna.

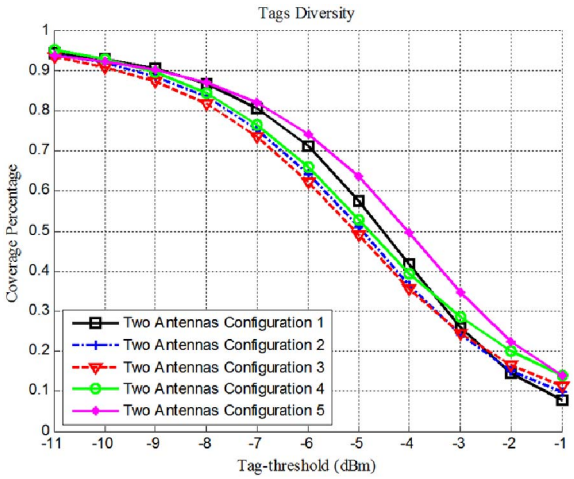

Fig. 13 Coverage performance of the 5 double antenna configurations, after the introduction of the proposed switch-controlled phase shift π.

References

[1] J. D. Griffin and G. D. Durgin, "Complete Link Budgets for Backscatter-Radio and RFID Systems," *IEEE Antennas Propagat. Magazine*, Vol. 51, No.2, April 2009.

[2] A. Lázaro, D. Girbau, D. Salinas, "Radio Link Budgets for UHF RFID on Multipath Environments," *IEEE Trans. Antennas Propagat.*, vol. 57, no. 4, April 2009.

[3] D. M. Dobkin, *The RF in RFID: Passive UHF RFID in Practice*. Newnes (Elsevier), 2008.

[4] A. C. Polycarpou, A. Dimitriou, A. Bletsas, J. N. Sahalos, "Radio Frequency Identification (RFID) for Healthcare," *COST ic0603* (*Antennas Systems & Sensors for Information Society Technologies*), Valencia, May 18-21 2009.

[5] S. R. Saunders, *Antennas and Propagation for Wireless Communication Systems*. John Wiley & Sons, 1999.

[6] C. A. Balanis, *Advanced Engineering Electromagnetics*. Chapter 5.5.2.D, 235—236, Wiley, 1989.

[7] O. Landron, M. J. Feuerstein, T. S. Rappaport, (1996) A comparison of theoretical and empirical reflection coefficients for typical exterior wall surfaces in a mobile radio environment. *IEEE Trans. Antennas Propagat.*, vol. 44, no. 3, pp. 341—351, March 1996.

[8] C. Oestges, B. Clerckx, L. Raynaud, and D. Vanhoenacker-Janvier, "Deterministic Channel Modeling and Performance Simulation of Microcellular Wide-Band Communication Systems", IEEE Trans. Veh Technol., vol. 51, no. 6, pp. 1422—1430, Nov. 2002.

[9] J-P. Curty, M. Declercq, C. Dehollain, N. Joehl, *Design and Optimization of Passive UHF RFID Systems*, Springer, 2007.

[10] A. Bletsas, A. G. Dimitriou, J. N. Sahalos, " Backscattering Improvement of UHF RFID Tag Efficiency," *International Workshop on Antenna Technology*, Lisbon, Portugal, March 2010.

[11] P.V. Nikitin, K. V. S. Rao, R. Martinez, and S. F. Lam, "Sensitivity and Impedance Measurements of UHF RFID Chips," *IEEE Trans. Microwave Theory & Techniques*, vol. 57, no. 5, part 2, May 2009.

[12] "UCODE G2XM and UCODE G2XL data sheet," NXP, Eindhoven, The Netherlands.

[13] "IPJ-P5002-D2 data sheet," Impinj, Seattle, Washington USA.

[14] "Higgs-3 data sheet", Allien, Morgan Hill, California, USA.

[15] J. D. Griffin, G. D. Durgin, A. Haldi, and B. Kippelen, "RF Tag Antenna Performance on Various Materials Using Radio Link Budgets," *IEEE Antennas & Wireless Propagation Letters*, vol. 5, pp. 247—250, 2006.